processes

MDPI

Article

Influences of the Braking Effect of Ruler EMBr on Molten Steel Flow and Steel–Slag Interface Fluctuation in a Continuous Casting Mold

Lin Xu [1,2,*], Qun-Wu Pei [3,*], Ze-Feng Han [2], Jie Cui [1], Hong-Gang Pan [1] and Yan-Tao Yao [4]

[1] Key Laboratory of Liaoning Province for Clean Combustion Power Generation and Heating Technology, Shenyang Institute of Engineering, Shenyang 110136, China
[2] Key Laboratory of Electromagnetic Processing of Materials, Northeastern University, Shenyang 110819, China
[3] Shenyang Academy of Instrumentation Science Co., Ltd., Shenyang 110043, China
[4] School of Environmental and Safety Engineering, Liaoning Petrochemical University, Fushun 113001, China
* Correspondence: lin_xu1989@163.com (L.X.); pei17692121221@163.com (Q.-W.P.)

Abstract: Electromagnetic braking (EMBr) technology, as one of the most effective technologies in the continuous casting process, provides an effective tool for improving the internal and external defects of steel products. Specifically, the EMBr technology takes the benefit of the generation of Lorentz force to decrease flow instability, mold powder entrapment, and surface defects, if applied properly. For this purpose, to gain a clear understanding of the effect of EMBr technology on the continuous casting process, a commonly used EMBr technology, namely ruler EMBr technology, is applied in the current work to investigate the dynamic behaviors of molten steel flow and steel–slag interface fluctuation inside a slab mold. Furthermore, to obtain a desirable braking effect of the ruler EMBr technology, operational parameters including the magnetic flux density, submerged entry nozzle (SEN) depth, and magnetic pole location are numerically investigated. The results demonstrate that the braking effect exerted by the ruler EMBr device is favorable for suppressing the impact of upward stream on the steel–slag interface with the magnetic flux density exceeding 0.3 T. For the influence of the SEN depth and magnetic pole location on the effect of ruler EMBr mold, the results show that a steady jet flow pattern can be obtained through the adjustment of a location between the ruler EMBr device and the SEN depth. For instance, when the ruler EMBr device installation position of 225 mm corresponds to the SEN depth of 150 mm, the upward deflection of jet stream is suppressed and a stable interface fluctuation profile is formed. With this adjustment, the possibility of mold flux entrapment is decreased.

Keywords: electromagnetic braking; continuous casting; molten steel flow; steel–slag interface fluctuation; mold

Citation: Xu, L.; Pei, Q.-W.; Han, Z.-F.; Cui, J.; Pan, H.-G.; Yao, Y.-T. Influences of the Braking Effect of Ruler EMBr on Molten Steel Flow and Steel–Slag Interface Fluctuation in a Continuous Casting Mold. *Processes* **2023**, *11*, 33. https://doi.org/10.3390/pr11010033

Academic Editor: Sara Liparoti

Received: 1 December 2022
Revised: 17 December 2022
Accepted: 21 December 2022
Published: 23 December 2022

1. Introduction

During continuous casting, the flow pattern of the melt in a mold is directly related to the quality of the slab [1–4]. Especially in a high-speed casting, a jet flow discharged from the submerged entry nozzle (SEN) rapidly impinges upon the mold narrow wall and splits into two violent backflows. The violent upward backflow moves upward along a casting direction and tends to form unstable fluctuations in the meniscus region. Such instability and fluctuation can induce entrapment of mold powder in an internal flow and irregular growth of an initial solidified shell on the slab mold wall [5]. Unlike the flow characteristics of upward backflow, the intensified downward backflow entrains nonmetallic inclusions and penetrates deeply into the mold. Such deep penetration can increase the difficulty of flotation separation of nonmetallic inclusions, resulting in deepening of vibration marks and the formation of transverse cracks [6–8]. Therefore, the problems induced by the disturbance behavior of molten steel inside the mold have a great impact on the surface and internal quality of the slab [9].

For a given slab caster, if the flow behavior of molten steel cannot be controlled within an optimal range, the disturbed flow of molten steel inside the mold will exist for a long time [5]. Hence, to obtain a stable continuous casting process, it is indispensable to optimize parameters related to the molten steel flow in the mold [10]. There have been many efforts to control the flow behavior of molten steel through optimizing of processing parameters, such as nozzle geometry, nozzle inclination angle, immersion nozzle depth, and continuous casting speed [11–13]. Another effective way, namely electromagnetic brake (EMBr) technology, has the potential to control the irregular flow behavior of molten steel within the mold as well if applied correctly [14]. The principle of EMBr technology is that a static magnetic field excited by a direct current restricts the flow of molten steel through certain regions of the mold. Within the certain regions, electromagnetic forces generated by the interaction between the electromagnetic field and the molten steel can be naturally adjusted according to flow variations, which makes it possible to obtain a reasonable flow control of the molten steel within the mold [5]. The studies of the effects of EMBr on the fluctuation behavior of steel–slag interface in the mold have confirmed this point as well [3,6,9].

Based on the principle of EMBr technique and the basic idea of controlling the flow of molten steel within the mold, there are two types of EMBr techniques commonly used in an industrial slab caster at present, namely ruler EMBr [15,16] and double ruler EMBr [17,18]. The distinguishing feature of the ruler EMBr is that a pair of horizontal magnetic poles located below the SEN ports completely cover the wide wall of the mold, aiming to restrict the impact of jet stream discharged from the SEN on the mold's narrow wall. However, due to the limitation of the horizontal magnetic pole location, the braking effect exerted by the ruler EMBr cannot be sufficient to restrain upward streams and stabilize surface fluctuations within the mold [19]. Hence, to strengthen the braking effect therein, the double ruler EMBr adds one more pair of magnetic poles horizontally arranged close to the top surface of the mold based on the ruler EMBr. In the same way, the horizontal magnetic poles of the double ruler EMBr extend to align with the entire wide wall of the mold. However, due to the existence of an additional pair of horizontal magnetic poles, the configuration of the double ruler EMBr is complicated and huge. In addition, if the double ruler EMBr is improperly applied, an excessive electromagnetic field will be produced near the top of the mold and, correspondingly, the flow of molten steel near the meniscus region will be excessively controlled. This can easily result in the formation of low temperature melt and the freezing of mold powder [20].

According to the above description, it is clear that the braking effect of EMBr technology has beneficial effects on the continuous casting process if applied correctly. In general, the braking effect exerted by the EMBr technology is greatly influenced by the processing and electromagnetic parameters [21]. By that, to achieve a desirable braking effect of the EMBr technology, the electromagnetic parameters should be matched with the variation of the processing parameters. This is because improper design of processing and electromagnetic parameters will result in the perturbed flow of molten steel not being effectively controlled and homogenized. Therefore, more extensive studies should be required to optimize the relevant parameters of the commonly used EMBr technology for molten steel flow under electromagnetic effect.

In this article, to optimize the dynamic behaviors of the molten steel flow and steel–slag two–phase interface fluctuation inside a slab mold, the braking effect of commonly used ruler EMBr technology under various electromagnetic and processing parameters, including the magnetic flux density, immersion nozzle depth, and magnetic pole location are numerically investigated in detail. The structural arrangement of this article is considered as follows. Section 2 provides the mathematical formulations and presents the details of the used numerical method. Section 3 presents the physical model of the ruler EMBr. The computational model is validated in Section 4 and the simulations results are discussed in Section 5. Eventually, the main conclusions are made in Section 6.

2. Mathematical Formulations and Conditions

To investigate the two–phase flow behavior of molten steel and mold flux within the mold, a three-dimensional (3-D) unsteady multi-field coupling mathematical model is established. During that numerical simulation process, to better monitor the two–phase interface fluctuation behavior of steel–slag within the mold, the assumptions are made as follows. The mold flux is considered to be liquid, and the influence of slag layers in other states is ignored. The molten steel and mold flux are regarded as homogeneous incompressible Newtonian fluid with constant physical properties. The effects of the oscillation of mold and negative taper on the molten steel flow state are not taken into account. In addition, the heat transfer, solidification and related thermal behaviors in the mold are neglected. On this basis, mathematical formulations in this paper can be described as below.

2.1. Mathematical Formulations

Two–Phase Flow Equation

The volume of fluid (VOF) method is adopted to establish a two–phase turbulent transient flow model, which can track the deformation of the steel–slag two–phase interface in a slab casting mold [14]. In the VOF method, the function of fluid volume in a space lattice can be defined through a moving steel–slag interface. The volume fraction of the molten steel in the mold can be obtained by the following equation.

$$\frac{\partial \Phi}{\partial t} + \nabla \Phi v_i = 0 \tag{1}$$

where, Φ equal to 1 represents the molten steel, Φ equal to 0 represents the mold flux, and Φ between 0 and 1 represents the two–phase interface.

In the research, because the molecules of the molten steel and mold flux attract each other in the mold, the interfacial tension can be formed at the steel–slag two–phase interface. In this study, the interfacial tension is solved by the continuum surface force (CSF) model proposed by Brackbill et al. [22]. Moreover, a volume force as a source term is added to the momentum equation to consider the interfacial tension effect. The expression is as follows.

$$F_{\mathrm{Vol},i} = \sigma \frac{\rho \kappa \nabla \Phi}{0.5(\rho_{\mathrm{st}} + \rho_{\mathrm{sl}})} \tag{2}$$

$$\rho = \rho_{\mathrm{st}} \Phi + \rho_{\mathrm{sl}} (1 - \Phi) \tag{3}$$

$$\kappa = \nabla \cdot \left(\frac{\nabla \Phi}{|\Phi|} \right) \tag{4}$$

Continuity equation

$$\frac{\partial (\rho v_i)}{\partial x_i} = 0 \tag{5}$$

Momentum equation

$$\frac{\partial (\rho v_i)}{\partial t} + \frac{\partial (\rho v_i v_j)}{\partial x_j} = -\frac{\partial p}{\partial x_i} + \frac{\partial}{\partial x_j} \left[\mu_{\mathrm{eff}} \left(\frac{\partial v_i}{\partial x_j} + \frac{\partial v_j}{\partial x_i} \right) \right] + \rho g_i + F_{M,i} + F_{\mathrm{Vol},i} \tag{6}$$

where,

$$\mu_{\mathrm{eff}} = \mu_l + \mu_t \tag{7}$$

$$\mu_l = \mu_{\mathrm{st}} \Phi + \mu_{sl} (1 - \Phi) \tag{8}$$

SST k-ω turbulence model equation

In the research, to improve the reliability of calculation, the Reynolds-averaged Navier–Stokes (RANS) SST k-ω model is performed to investigate the flow characteristics between the molten steel and mold flux within the mold [14]. In comparison with the other two-

equation turbulence models, the most remarkable feature of the SST k-ω model is that it considers a mixing function to better reflect the effect of the Reynolds stress on the flow behavior of molten steel in the near-wall region [23,24]. In this region, an automatic wall function can be freely converted between high and low Reynolds numbers, so that the molten steel flow pattern under the engineering situation can be better obtained. The expressions of two-equation turbulence model are expressed as follows.

$$\frac{\partial(\rho k)}{\partial t} + v_j \frac{\partial(\rho k)}{\partial x_j} = \frac{\partial}{\partial x_j}\left[\left(\mu + \frac{\mu_t}{\sigma_k}\right)\frac{\partial k}{\partial x_j}\right] + G_k - Y_k \tag{9}$$

$$\frac{\partial(\rho \omega)}{\partial t} + v_j \frac{\partial(\rho \omega)}{\partial x_j} = \frac{\partial}{\partial x_j}\left[\left(\mu + \frac{\mu_t}{\sigma_\omega}\right)\frac{\partial \omega}{\partial x_j}\right] + G_\omega - Y_\omega + D_\omega \tag{10}$$

where,

$$\sigma_k = \frac{1}{F_1/\sigma_{k,1} + (1 - F_1)/\sigma_{k,2}} \tag{11}$$

$$\sigma_\omega = \frac{1}{F_1/\sigma_{\omega,1} + (1 - F_1)/\sigma_{\omega,2}} \tag{12}$$

$$G_k = \mu_t \left\{ 2\left[\left(\frac{\partial v_i}{\partial x_i}\right)^2 + \left(\frac{\partial v_j}{\partial x_j}\right)^2\right] + \left(\frac{\partial v_i}{\partial x_j} + \frac{\partial v_j}{\partial x_i}\right)^2 \right\} \tag{13}$$

Electromagnetic field model

To investigate the electromagnetic field characteristics in the mold, the magnetic induction method derived from Ohm's law and Maxwell's equation is employed [25]. In computational procedure, the generation of electromagnetic force is induced by the interaction of flowing molten steel with externally applied magnetic field. Based on the externally applied magnetic field $B_{0,i}$, the induced magnetic field b_i is obtained by the following equation.

$$\frac{\partial b_i}{\partial t} + (v_i \cdot \nabla) b_i = \frac{1}{\mu\sigma}\nabla^2 b_i + [(B_{0,i} + b_i)\cdot\nabla]v_i - (v_i \cdot \nabla)B_{0,i} \tag{14}$$

The induced current density J_i is given by as follows.

$$J_i = \frac{1}{\mu}\nabla \times B_i = \frac{1}{\mu}\nabla \times (B_{0,i} + b_i) \tag{15}$$

The electromagnetic force $F_{m,i}$ as additional force in the momentum equation is obtained by the following equation.

$$F_{m,i} = J_i \times B_i = J_i \times (B_{0,i} + b_i) \tag{16}$$

2.2. Computational Conditions

The inlet is positioned at the top of the SEN, which is defined as a velocity inlet boundary condition. Moreover, the inlet velocity is calculated based on a specific casting speed to preserve the flow equilibrium. The top surface of the mold defined as a symmetrical boundary condition is a free surface, where the normal gradients of velocity component and other variables perpendicular to the free surface are set to a value of zero [14]. The central plane of mold width is a symmetrical plane with the same boundary condition as the free surface [21]. The mold wall is defined as the boundary condition of the non-slip insulation wall, in which the normal component of induced current and the normal gradients of other variables are set to a value of zero [23]. Moreover, an automatic near wall treatment is performed by the SST k-ω turbulence model. The bottom of the computational domain is set as a mold exit, which is defined as an outflow condition with fully developed flow. At

the bottom of the computational domain, the normal gradients of all variables are set to a value of zero [14].

The boundary condition for the induced magnetic field b_i is given by [14]:

$$b_i = \{b_n \quad b_{t1} \quad b_{t2}\}^T \tag{17}$$

where the subscripts represent the normal and tangential components of the field.

During continuous casting, the mold flux with non-conductive properties sometimes penetrates into the channel between the mold wall and the solidified shell to reduce withdrawal forces. Hence, the mold wall can be regarded as an insulating wall. Correspondingly, an electrically insulating boundary condition is employed in the calculation of the electromagnetic field. For this purpose, b_{t1} and b_{t2}, which are tangential components of the field, should satisfy the following conditions.

$$b_{t1} = b_{t2} = 0 \tag{18}$$

3. Geometric Configurations

3.1. Ruler EMBr Configuration

The ruler EMBr configuration installed in the mold is shown in Figure 1. The cross section of the mold is 1450 mm × 230 mm, and the height of the mold is 800 mm. As can be seen, the ruler EMBr configuration consists of a pair of horizontal magnetic poles, which cover the whole wide faces of the mold. In detail, the horizontal magnetic poles with two sets of electrified coils are installed below the SEN to suppress the excessive penetration of jet flow discharged from the SEN into the molten pool.

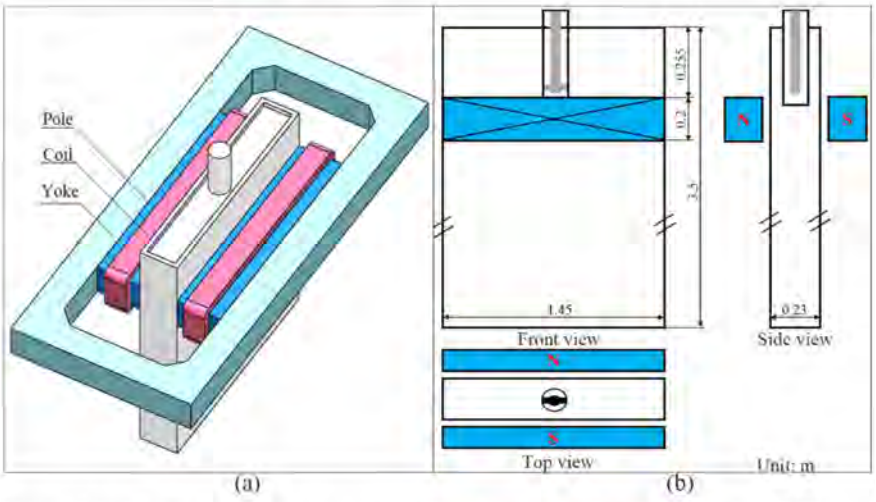

Figure 1. Schematic diagram of ruler EMBr device: (**a**) schematic of ruler EMBr device and (**b**) plane view of ruler EMBr device.

3.2. Computational Domain and Parameters

The schematic of the computational domain is shown in Figure 2. Due to the geometric symmetry, a one-half volume of the mold is considered (see Figure 2a). To ensure the grid quality of mold, a hexahedral structured meshing method is performed. To improve the computing accuracy, a local mesh refinement method is employed in the region close to the mold wall and the steel–slag two–phase interface (see Figure 2b). Moreover, the computational domain is extended to 3500 mm to ensure the full development of the flow of molten steel in the mold. The operating and physical parameters related to the present calculation are shown in Table 1.

Figure 2. Schematic diagram of mold computational domain: (**a**) geometry of mold and (**b**) mesh of mold.

Table 1. Parameters of continuous casting slab mold used in numerical simulation.

Parameter	Value
Mold size	1450 mm × 230 mm
Effective mold length	800 mm
Computational domain	1450 mm × 230 mm × 3500 mm
Depth of SEN	130, 150, and 170 mm
Outlet section of SEN	65 mm × 80 mm
Angle port of SEN	−15°
Casting speed	1.6 m·min^{-1}
Molten steel density	7020 kg·m^{-3}
Molten steel viscosity	0.0056 Pa·s
Molten steel electric conductivity	7.14 × 10^{5} S·m^{-1}
Molten steel magnetic permeability	1.26 × 10^{-6} H·m^{-1}
Mold flux density	3500 kg·m^{-3} [3]
Mold flux viscosity	0.2664 Pa·s [3]
Liquid mold flux height	35 mm
Interface tension coefficient	1.2 N·m^{-1}
Magnetic flux density	0, 0.1, 0.2, 0.3, and 0.5 T
Magnetic pole position	225, 255, and 285 mm

4. Model Validation

In the current research, to validate the accuracy of the coupling calculation between the flow field and electromagnetic field, a simple 3D example performed by Cho et al. [26] and a description of available experimental data provided by Moreau [27] are employed. The simulation parameters of 3D plate are shown in Table 2. The velocity profiles of numerical simulation and experimental measurements are illustrated in Figure 3. As can be seen, the velocity distribution curves all present an "M-shaped" profile. That is to say, with the use of identical geometry and parameters, the numerical results solved by the author are in good agreement with those provided by other researchers [26,27]. In this article, the same numerical method is used to solve the coupling of the flow field and electromagnetic field.

Therefore, we conjecture that the current simulation research method on the coupling of the flow field and electromagnetic field has a relatively reasonable accuracy.

Table 2. Parameters of 3D plate used in numerical simulation.

Parameter	Value	Parameter	Value
Computational domain length	704 mm	Liquid viscosity	0.00155825 Pa·s
Computational domain height	40 mm	Liquid electric conductivity	1.05×10^6 S·m^{-1}
Computational domain thickness	2 mm	Liquid inlet velocity	1.16141 m·s^{-1}
EMBr central region length	304 mm	Inlet turbulent kinetic energy	5.99×10^5 m^2·s^{-2}
Magnetic flux density	1.3482 T	Turbulent dissipation rate	7.529×10^5 m^2·s^{-3}
Liquid density	13,550 kg·m^{-3}	Static pressure at exit	0

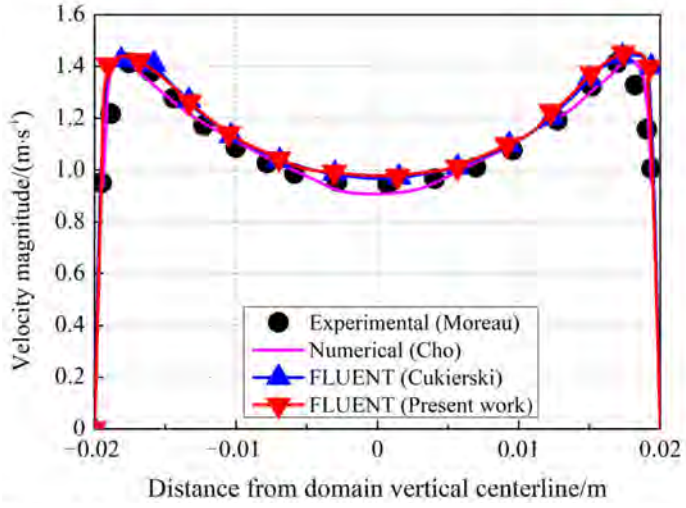

Figure 3. Velocity profiles along a vertical line at the horizontal center of MHD computational domain.

5. Results and Discussion

5.1. Electromagnetic Characteristics in Mold with Ruler EMBr

Distribution of electromagnetic performances in the mold with a magnetic flux density of 0.3 T is shown in Figure 4. As shown in Figure 4a, with ruler EMBr, the maximum magnetic flux density reaches 0.26 T in the jet impingement region, while the respective value at the mold exit is only 0.02 T. As shown in Figure 4b, the current density is mainly induced in the jet impingement region, and the vortices of induced current are formed at the region where the jet stream is divided into an upward backflow and a downward backflow. As shown in Figure 4c, the electromagnetic force produces a braking effect directly on the jet flow discharged from the SEN. Hence, the traditional ruler EMBr technology shows the potential to suppress the impact strength of the jet stream on the molten pool.

5.2. Molten Steel Flow Characteristics in Mold with the Variation of Magnetic Flux Density

To evaluate the braking effect of ruler EMBr, in the following we numerically analyze the dynamic behaviors of the molten steel flow and steel–slag two–phase interface fluctuation in the mold. In this section, all other parameters remain the same except for the change in magnetic flux density. The following constant parameters are assumed: a casting speed (V_C) of 1.6 m/min, a SEN depth (D_{SEN}) of 150 mm, and an installation position (H) of the ruler EMBr device at a distance of 255 mm from the top of the mold.

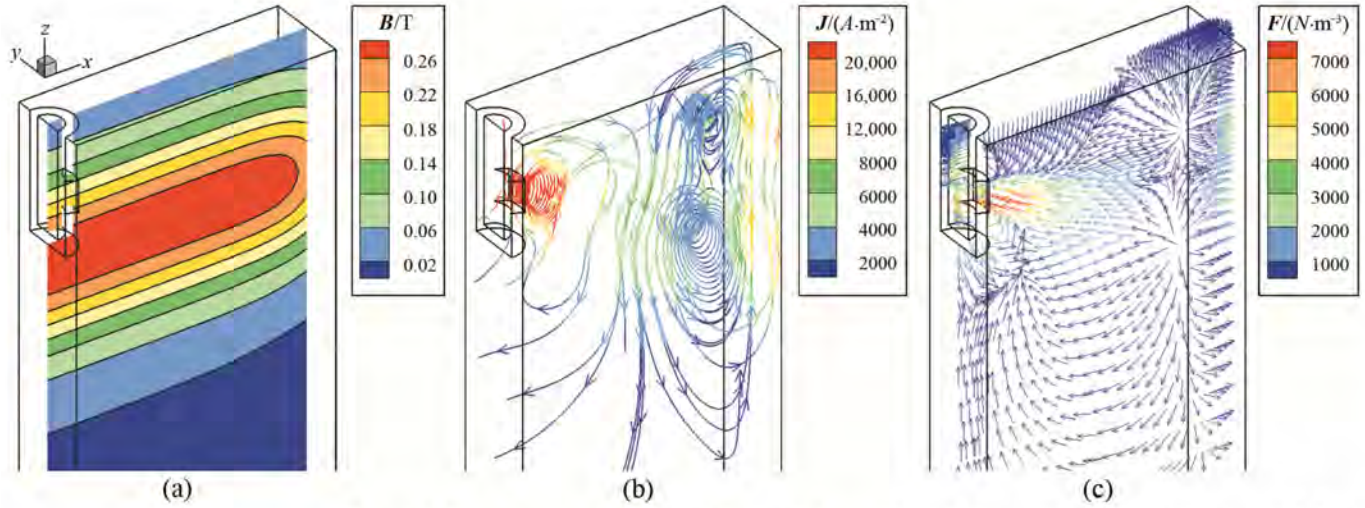

Figure 4. Electromagnetic characteristics in the mold with the magnetic flux density of 0.3 T: (**a**) magnetic flux density, (**b**) induced current density, and (**c**) electromagnetic force.

Figure 5 presents the flow field of molten steel in the centre of the mold wide face with various magnetic flux densities. As shown in Figure 5a, with no EMBr, the jet flow discharged from the SEN rapidly impinges on the mold narrow face, and then splits into two high-speed backflows, i.e., an upward backflow and a downward backflow. As shown in Figure 5b,c, with a magnetic flux density of 0.1 and 0.2 T, the braking effect exerted by the ruler EMBr is not significant. A violent upward backflow is formed in the upper recirculation region of the mold. However, as shown in Figure 5d,e, with an increase in the magnetic flux density, the braking effect of the ruler EMBr on the jet flow is obviously enhanced. Especially for a magnetic flux density of 0.5 T, the fluidity of the additional vortex and the tilt upward characteristic of the jet flow are obviously increased. As can be seen, the jet flow in the action region of magnetic pole is pushed away by the electromagnetic force. Afterwards, the core of the vortex moves upward in the upper recirculation region of the mold. In the lower recirculation region of the mold, in turn, an additional vortex is formed.

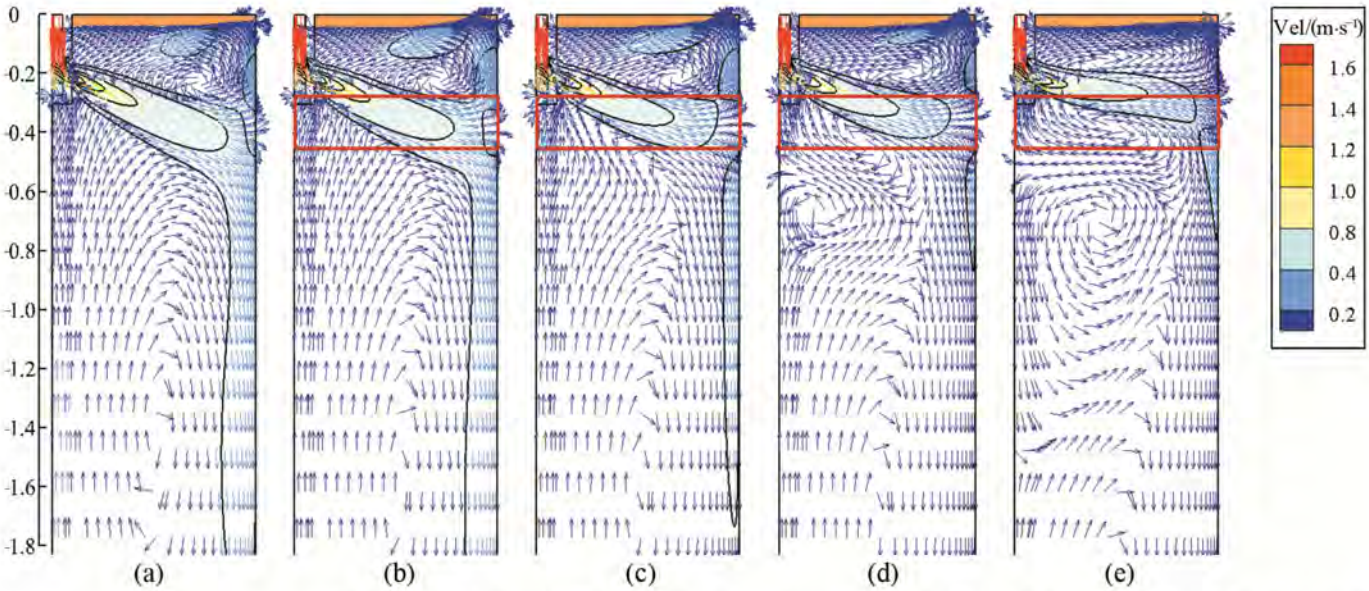

Figure 5. Distribution of the molten steel flow field in the central plane of the mold thickness with various magnetic flux densities: (**a**) B_{max} = 0 T, (**b**) B_{max} = 0.1 T, (**c**) B_{max} = 0.2 T, (**d**) B_{max} = 0.3 T and (**e**) B_{max} = 0.5 T.

Figure 6 illustrates the 3D steel–slag two–phase interface profiles in the mold with different magnetic flux densities. In detail, the steel–slag two–phase interface is represented by the volume fraction of mold flux Φ = 0.5. With the application of ruler EMBr, increasing the magnetic flux density to 0.2 T cannot significantly control the fluctuation of the steel–slag two–phase interface. On the contrary, when the magnetic flux density increases to 0.3 T, the deformation of the steel–slag two–phase interface tends to be stable. Particularly for the magnetic flux density increases to 0.5 T, the steel–slag interface fluctuation is effectively controlled, and the maximum meniscus fluctuation height is decreased to 9.4 mm.

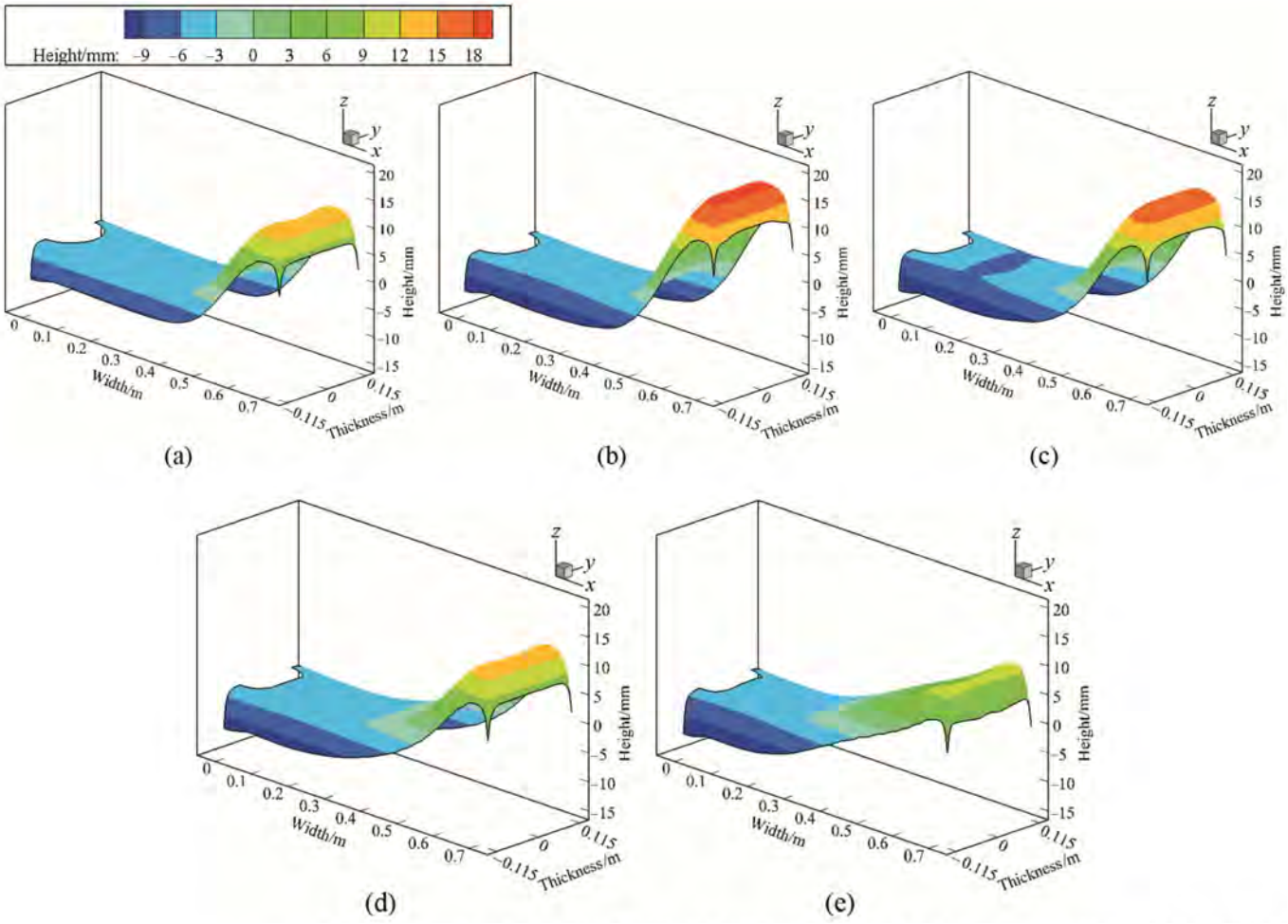

Figure 6. Steel–slag two–phase interface fluctuation profiles in the mold with various magnetic flux densities: (**a**) B_{max} = 0 T, (**b**) B_{max} = 0.1 T, (**c**) B_{max} = 0.2 T, (**d**) B_{max} = 0.3 T and (**e**) B_{max} = 0.5 T.

To quantitatively analysis the effect of the magnetic flux density on the molten steel velocity within the mold, the profiles of the molten steel velocity at the steel–slag two–phase interface (Y = 0 m, Z = −0.035 m) and molten steel vertical velocity close to the mold narrow face (X = 0.695 m, Y = 0 m) are shown in Figure 7. As can be seen, the maximum amplitude of the surface velocity increases from 0.18 to 0.20 m/s as the magnetic flux density increases from 0 to 0.2 T (see Figure 7a). Correspondingly, the maximum amplitude of vertical velocity increases from 0.24 to 0.25 m/s in the upper recirculation region of the mold (see Figure 7b). Such results imply that the braking effect exerted by the ruler EMBr is insufficient to suppress the flow of molten steel in the upper recirculation region of the mold, with the magnetic flux density increasing to 0.2 T. In comparison, when the magnetic flux density increases from 0.3 to 0.5 T, the braking effect exerted by the ruler EMBr on the upward backflow is meaningful. The maximum amplitude of the surface velocity and vertical velocity of molten steel in the upper recirculation region of the mold are significantly decreased to 0.12 and 0.11 m/s, respectively.

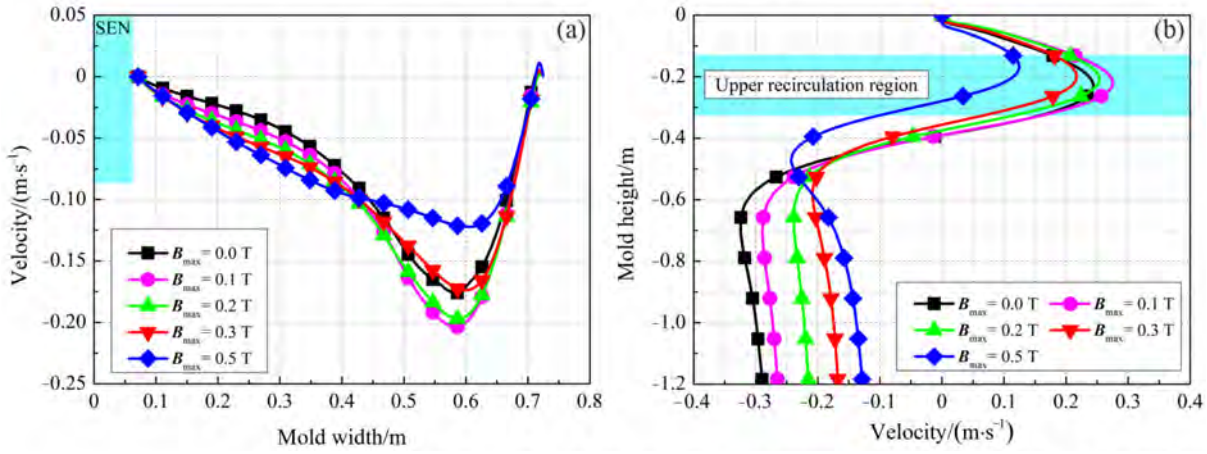

Figure 7. Velocity profiles in the mold with various magnetic flux densities: (**a**) steel–slag interface velocity (Y = 0 m, Z = −0.035 m) and (**b**) vertical velocity along mold height direction (X = 0.695 m, Y = 0 m).

Figure 8 shows the influence of the magnetic flux density on the distribution of turbulent kinetic energy close to the mold narrow face (X = 0.695 m). As can be seen, with no EMBr, the maximum turbulent kinetic energy is concentrated in the jet impingement region. Similar findings can also be found in the application of ruler EMBr. As the ruler EMBr is applied, increasing the magnetic flux density from 0.1 to 0.3 T can enhance the braking effect in the molten steel flow. Correspondingly, a reduced turbulent kinetic energy is obtained in the jet impingement region. However, when the magnetic flux density continues to increase to 0.5 T, the braking effect exerted by the ruler EMBr can induce an upward tilting jet flow to frequently impact the narrow surface of mold. This finding can be found in the braking effect of ruler EMBr on the upward backflow in the mold, see Figure 5e. By that, with the support of 0.5 T, a slight increase in turbulent kinetic energy is formed in the jet impingement region. Even so, a noticeable reduction in turbulent kinetic energy occurs near the meniscus region when compared to the cases of 0.2 and 0.3 T. The results indicate that the ruler EMBr shows the beneficial effects of restraining the meniscus surface flow as the magnetic flux density increases to 0.5 T.

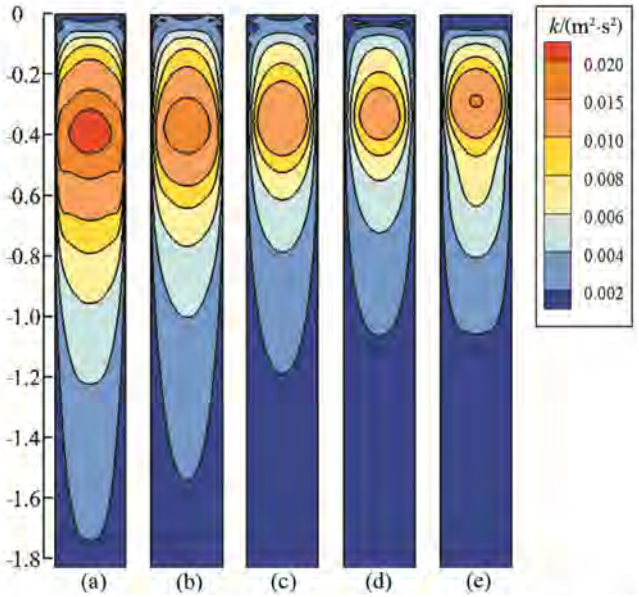

Figure 8. Turbulent kinetic energy distribution close to the mold narrow face with various magnetic flux densities: (**a**) B_{max} = 0 T, (**b**) B_{max} = 0.1 T, (**c**) B_{max} = 0.2 T, (**d**) B_{max} = 0.3 T and (**e**) B_{max} = 0.5 T.

5.3. Molten Steel Flow Characteristics in Mold with the Variation of SEN Depth

In the traditional ruler EMBr technology, operational parameters, including the SEN port angle, SEN depth, and casting speed, etc., are crucial in affecting the molten steel flow within the mold. In this section, we tend to investigate the influence of dynamic behaviors of the molten steel flow and steel–slag tow–phase interface fluctuation within the mold with the variation of SEN depth. The standard process parameters are performed with a casting speed of 1.6 m/min, a magnetic flux density of 0.3 T, and an installation position of the ruler EMBr device at a distance of 255 mm from the top of the mold.

In the previous section, we find that the braking effect exerted by the ruler EMBr effectively restrains the impact of the impinging jet flow to the molten pool when the magnetic flux density exceeds 0.3 T. Correspondingly, two backflows, i.e., an upward backflow and a downward backflow within the mold are well controlled and, hence, are not considered for further analysis in the follow-up research work. Figure 9 shows the influence of SEN depth on the flow of molten steel within the mold with a fixed magnetic flux density of 0.3 T. Among these graphs, each of the subgraphs located above the black horizontal dividing line indicates the contours of the molten steel velocity magnitude at the steel–slag tow–phase interface. Conversely, below the black horizontal dividing line, each of the subgraphs represents the predicted flow fields in the central plane of the mold. As can be seen, with an increase in the depth of SEN, the horizontal poles action region can well cover the main jet stream discharged from the nozzle–exit. This considerably contributes to the formation of a downward deflection of jet stream. Hence, in the case of the SEN depth of 170 mm, the distance of the upward backflow to the steel–slag interface is prolonged. According to the law of mass conservation, the kinetic energy consumed by the upward backflow increases. Correspondingly, a reduced molten steel flow velocity appears at the steel–slag tow–phase interface, which contributes to stabilize the interface fluctuation in this case.

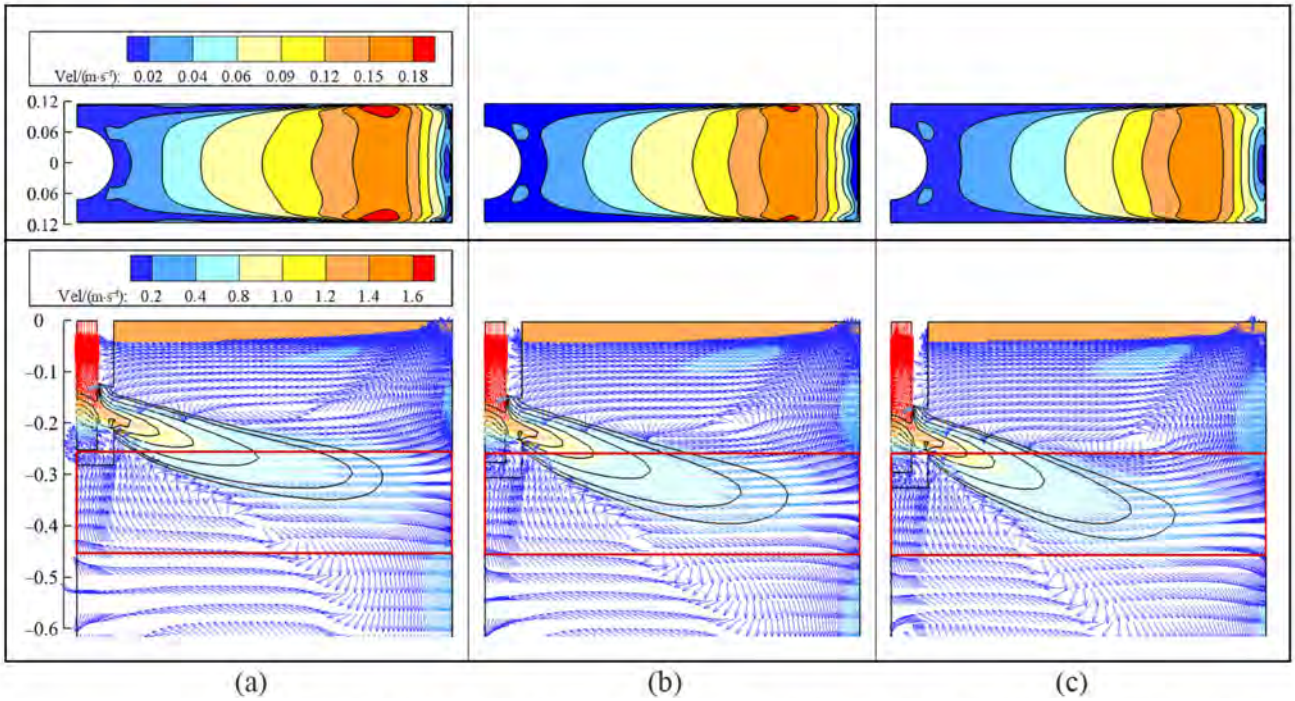

Figure 9. Molten steel flow characteristics in the mold with ruler EMBr under different SEN depths: (**a**) D_{SEN} = 130 mm, (**b**) D_{SEN} = 150 mm, and (**c**) D_{SEN} = 170 mm.

Figure 10 shows the influence of the SEN depth on the steel–slag tow–phase interface fluctuations within the mold with a fixed position of the ruler EMBr device. As discussed before, we find that with the increase of the SEN depth, the distance between the lower surface of the SEN and the upper surface of the horizontal magnetic poles decreases. As

a result, the main jet stream is concentrated in a high magnetic field region. That is, the braking effect is increased therein, and the molten steel flow velocity at the steel–slag tow–phase interface is correspondingly decreased. In our simulation, for a given fixed position of the ruler EMBr device, when the distance between the upper surface of the ruler EMBr device and the top of the mold is 255 mm, a stable interface fluctuation within the mold is obtained in the case of the SEN depth of 170 mm. As can be seen, as the SEN depth increases from 130 to 170 mm, the maximum amplitude of the steel–slag tow–phase interface fluctuation decreases from 14.7 to 12.8 mm, which decreases by 12.9 pct.

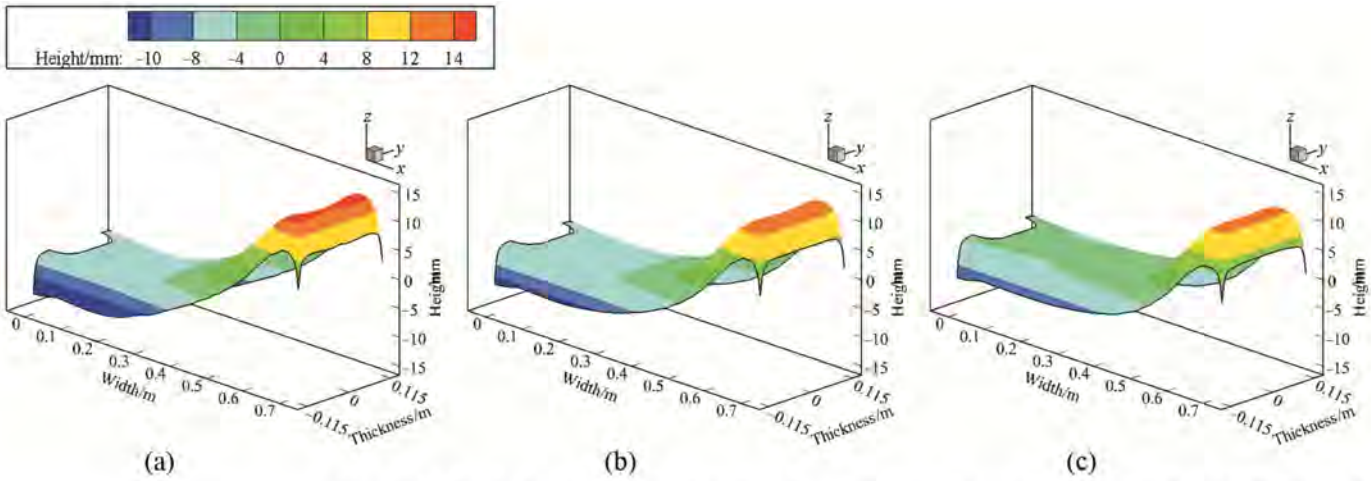

Figure 10. Steel–slag two–phase interface fluctuation profiles in the mold with ruler EMBr under different SEN depths: (**a**) D_{SEN} = 130 mm, (**b**) D_{SEN} = 150 mm, and (**c**) D_{SEN} = 170 mm.

In the electromagnetic continuous casting process, the molten steel flow pattern within the mold is susceptible to the variation of the SEN depth, especially in the application of the traditional ruler EMBr technology. For this purpose, it is essential to quantitatively investigate the influence of the SEN depth on the molten steel flow within the mold under the condition of a fixed installation position of the ruler EMBr device. Figure 11 shows the profiles of the velocity and turbulent kinetic energy of molten steel near the narrow face of the mold (X = 0.695 m, Y = 0 m) with various SEN depths. As can be seen, for the ruler EMBr device with a distance of 255 mm below the top of the mold, as the SEN depth increases from 130 to 170 mm, the maximum vertical velocity in the upper recirculation region of the mold decreases from 0.25 to 0.18 m/s, and the maximum turbulent kinetic energy in the impingement region obviously decreases from 0.02 to 0.01 m^2/s^2. Such results imply that the ruler EMBr device with a SEN depth of 170 mm can achieve the best performance in suppressing the upward backflow compared to the SEN depths of 130 and 150 mm.

5.4. Molten Steel Flow Characteristics in Mold with the Variation of Ruler EMBr Position

In our simulation, when the magnetic flux density exceeds 0.3 T, we find that the application of ruler EMBr can restrain the upward stream and reduce the surface molten steel flow, subsequently affecting the meniscus fluctuation in the mold. In the following part, to further explore the metallurgical effect of ruler EMBr with the variation of magnetic pole position, we continue to conduct numerical analysis on the dynamic behaviors of the molten steel flow and steel–slag interface fluctuation within the mold. During the numerical calculation process, only the following constant parameters are considered: a casting speed of 1.6 m/min, a SEN depth of 150 mm, and a magnetic flux density of 0.3 T.

Figure 12 shows the influence of ruler EMBr position on the flow of molten steel within the mold. As can be seen from the subgraphs below the horizontal dividing line, with the variation of the position of horizontal magnetic poles, the flow pattern of the molten steel in the mid-plane of the mold is similar. Breaking away from the constraint of nozzle–exit,

the jet flow propagates into the mold, forming a typical double-roll flow. However, the distortion of jet flow changes significantly. With the horizontal poles moving down, the jet flow deforms and deflects upward. Correspondingly, an inherently unstable flow is formed at the steel–slag two–phase interface. This is due to the fact that the braking effect exerted by the ruler EMBr is far away from the jet flow discharged from the nozzle–exit. Hence, the suppression of jet flow is weakened, and then the impact of upward backflow on the top of the mold is increased. As can be seen from the subgraphs above the horizontal dividing line, when the horizontal poles move down to a distance of 285 mm from the top of the mold, the maximum amplitude of steel–slag interface velocity increases to 0.18 m/s.

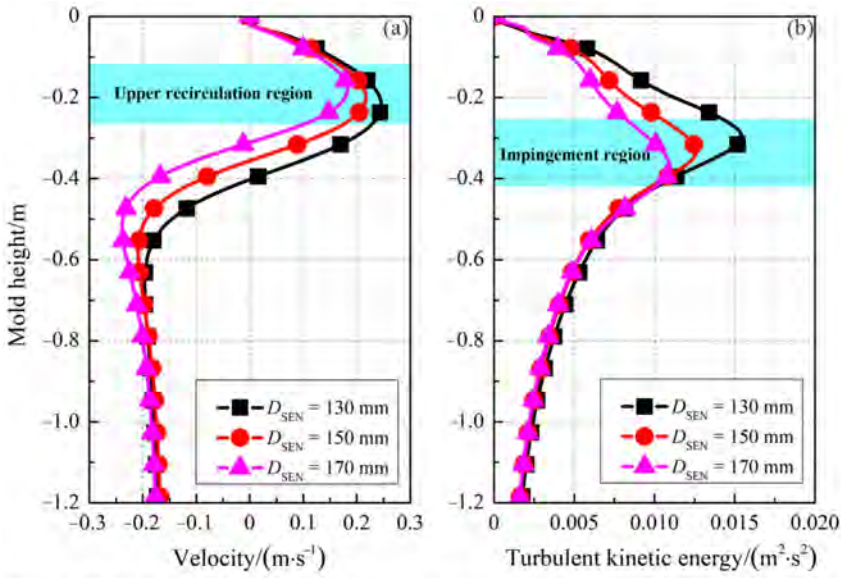

Figure 11. Velocity and turbulent kinetic energy profiles along mold height direction (X = 0.695 m, Y = 0 m) with ruler EMBr under different SEN depths: (**a**) vertical velocity and (**b**) turbulent kinetic energy.

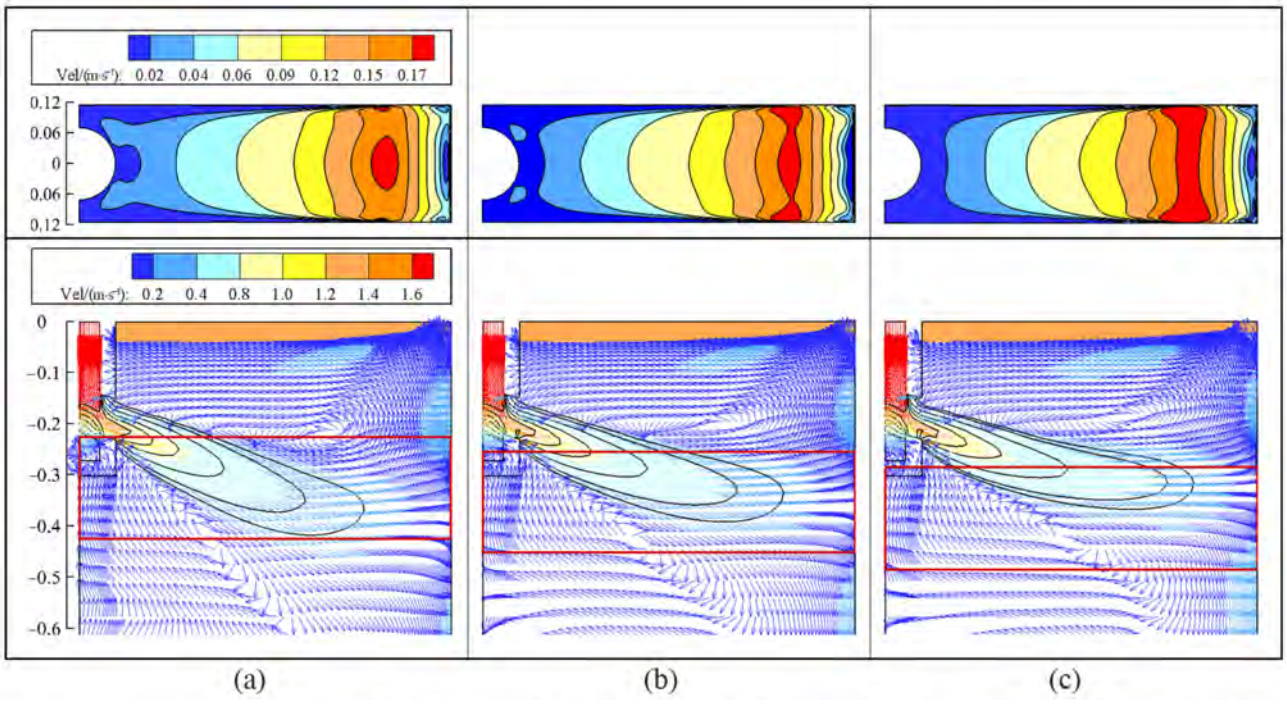

Figure 12. Molten steel flow characteristics in the mold with different positions of the ruler EMBr: (**a**) H_1 = 225 mm, (**b**) H_2 = 255 mm, and (**c**) H_3 = 285 mm.

Through the adjustment of a location between the ruler EMBr device and the SEN depth, a relatively steady steel–slag interface profile can be obtained, as expected. Figure 13 shows the effect of the ruler EMBr position on the steel–slag two–phase interface fluctuations within the mold with a fixed SEN depth of 150 mm. As mentioned above, the braking effect of ruler EMBr on the jet stream discharged from the nozzle–exit is weakened with the horizontal magnetic poles moving down. Hence, the upward backflow accelerates to move to the top of the mold, and correspondingly forms a relatively active steel–slag interface profile. As can be seen, with the support of 0.3 T, the maximum amplitude of the steel–slag two–phase interface fluctuation is 13.5, 13.8, and 14.8 mm in turn when the distance between the upper surface of the ruler EMBr device and the top of the mold is fixed to 225, 255, and 285 mm, respectively. To summarize, the numerical results indicate that a higher braking effect exerted by the ruler EMBr exists when the upper surface of the ruler EMBr device is positioned in a distance of 225 mm below the top of the mold.

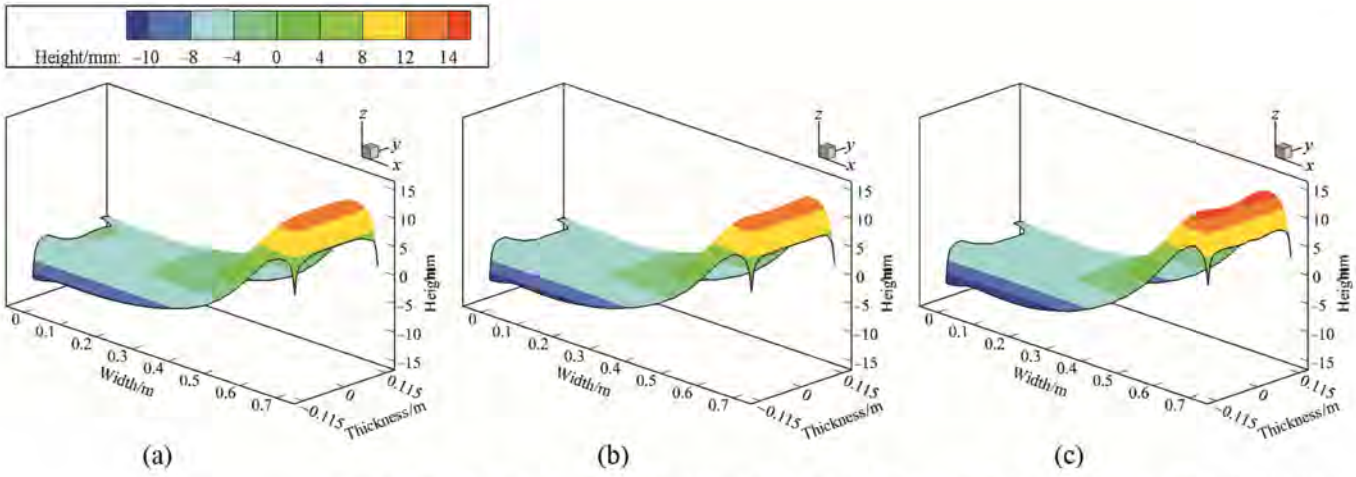

Figure 13. Steel–slag two–phase interface fluctuation profiles in the mold with various positions of the ruler EMBr: (**a**) H_1 = 225 mm, (**b**) H_2 = 255 mm, and (**c**) H_3 = 285 mm.

To quantitatively analyse the influence of the installation position of the ruler EMBr device on the flow of molten steel in the mold with a fixed depth of SEN, the profiles of the velocity and turbulent kinetic energy of molten steel near the narrow face of the mold (X = 0.695 m, Y = 0 m) are illustrated in Figure 14. As can be seen, in the case of the ruler EMBr device position of H_1 = 225 mm, the amplitude of molten steel velocity in the upper recirculation region of the mold is reduced, resulting in a decreased turbulent kinetic energy therein. This showed that the braking effect of the ruler EMBr in the case of H_1 = 225 mm is more effective than that in the case of H_2 = 255 mm and H_3 = 285 mm. This is due to the fact that the distance between the SEN depth and the ruler EMBr device position is relatively appropriate. Therefore, the main jet stream can concentrate within the horizontal poles action region. By that, the braking effect exerted by the ruler EMBr is correspondingly strengthened.

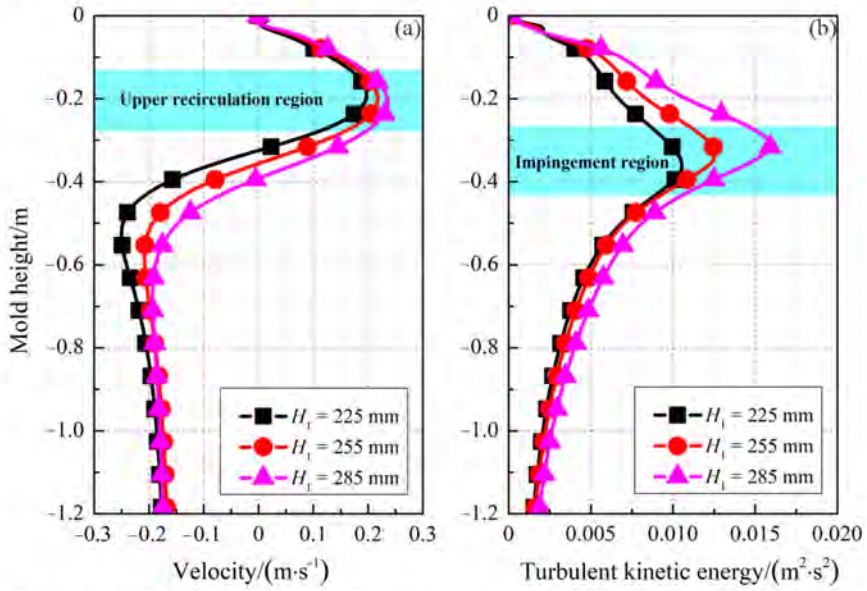

Figure 14. Velocity and turbulent kinetic energy profiles along mold height direction (X = 0.695 m, Y = 0 m) with different positions of the ruler EMBr: (**a**) vertical velocity and (**b**) turbulent kinetic energy.

6. Conclusions

In this article, a systematic numerical simulation was performed to investigate the braking effect of the traditional ruler EMBr technology under different operating parameters, including the magnetic flux density, SEN depth, and ruler EMBr device installation position. The main conclusions are summarized as follows.

1. With the application of the ruler EMBr in the mold, a steady magnetic field is concentrated in the jet impingement region and, correspondingly, a strong electromagnetic force is generated therein. As a result, the jet flow discharged from the nozzle–exit is directly suppressed by the electromagnetic force applied by the ruler EMBr device.
2. When the magnetic flux density exceeds 0.3 T, a favorable prognostic factor of the ruler EMBr device is that the braking effect can restrain the impact of upward backflow on the free surface of the mold. This benefit can contribute to stabilize the interface fluctuation and prevent the mold flux entrapment. For instance, with a magnetic flux density of 0.5 T, the maximum amplitude of steel–slag interface fluctuation decreases by 33.3 pct when compared to the case of no EMBr.
3. When the ruler EMBr device location remains fixed, the impact strength of the jet flow decreases with an increase of SEN depth. Specifically, for a fixed ruler EMBr device position of 255 mm, a desirable braking effect can be obtained at a SEN depth of 170 mm. With this adjustment, the maximum amplitude of the vertical velocity in the upper recirculation region of the mold decreases by 28 pct compared to a SEN depth of 130 mm.
4. An increased distance between the ruler EMBr device location and the top of the mold results in a reduced braking effect on the jet stream at a constant SEN depth. Correspondingly, a relatively active steel–slag interface profile is formed. In detail, for a given SEN depth of 150 mm, when the ruler EMBr device is located at 285 mm, the maximum amplitude of the steel–slag two–phase interface fluctuation increases by 9.6 pct compared to the ruler EMBr device located at 225 mm.

Author Contributions: Conceptualization, L.X. and Q.-W.P.; validation, L.X. and Z.-F.H.; formal analysis, L.X. and Z.-F.H.; investigation, L.X. and J.C.; writing—original draft preparation, L.X.; writing—review and editing, L.X., J.C., H.-G.P. and Y.-T.Y.; project administration, L.X.; funding acquisition, L.X. All authors have read and agreed to the published version of the manuscript.

Funding: This research was funded by the National Natural Science Foundation of China (No. 51901095), the Scientific Research Project of Liaoning Provincial Department of Education (No. LJKQZ20222282), and the Natural Science Foundation of Liaoning Province (Nos. 2022-BS-224 and 2022-MS-304).

Data Availability Statement: Not applicable.

Acknowledgments: The authors thank the referees for their work, which greatly contributed to this article.

Conflicts of Interest: The authors declare no conflict of interest.

Nomenclature

p	pressure, [Pa]
v_j	steel velocity, [m·s^{-1}]
g_i	gravitational acceleration, [m^2·s^{-1}]
$F_{\mathrm{Vol},i}$	interaction force, [N·m^{-3}]
$F_{\mathrm{m},i}$	electromagnetic force, [N·m^{-3}]
J_i	eddy current density, [A·m^{-2}]
b_i	induced magnetic field, [T]
$B_{0,i}$	applied magnetic field, [T]
G_k	generation of turbulence kinetic energy
G_ω	generation of specific dissipation rate
Y_k	dissipation of turbulent kinetic energy
Y_ω	dissipation of specific dissipation rate
D_ω	cross diffusion
F_1	blending function
Greek symbols	
ρ	density, [kg·m^{-3}]
ρ_{st}	steel density, [kg·m^{-3}]
ρ_{sl}	mold flux density, [kg·m^{-3}]
μ_{eff}	effective viscosity, [kg·m^{-1}·s^{-1}]
μ_{l}	laminar viscosity, [kg·m^{-1}·s^{-1}]
μ_{t}	turbulent viscosity, [kg·m^{-1}·s^{-1}]
μ_{st}	steel laminar viscosity, [kg·m^{-1}·s^{-1}]
μ_{sl}	mold flux laminar viscosity, [kg·m^{-1}·s^{-1}]
Φ	volume fraction of steel
κ	mean surface curvature
σ_k	turbulent Prandtl number
σ_ω	turbulent Prandtl number
k	turbulent kinetic energy, [m^2·s^{-2}]
ω	turbulent dissipation rate, [s^{-1}]
σ	steel electrical conductivity, [S·m^{-1}]
Subscripts	
eff	effective
M	magnetic
Vol	volume
l	laminar
t	turbulent
st	steel
sl	slag

References

1. Liang, M.; Cho, S.M.; Ruan, X.; Thomas, B.G. Modeling of multiphase flow, superheat dissipation, particle transport, and capture in a vertical and bending continuous caster. *Processes* **2022**, *10*, 1429. [CrossRef]
2. Saldaña-Salas, F.; Torres-Alonso, E.; Ramos-Banderas, J.A.; Solorio-Díaz, G.; Hernández-Bocanegra, C.A. Analysis of the depth of immersion of the submerged entry nozzle on the oscillations of the meniscus in a continuous casting mold. *Metals* **2019**, *9*, 596. [CrossRef]
3. Deng, A.; Xu, L.; Wang, E.; He, J. Numerical analysis of fluctuation behavior of steel/slag interface in continuous casting mold with static magnetic field. *J. Iron Steel Res. Int.* **2014**, *21*, 809–816. [CrossRef]

4. Shen, B.; Shen, H.; Liu, B. Instability of fluid flow and level fluctuation in continuous thin slab casting mould. *ISIJ Int.* **2007**, *47*, 427–432. [CrossRef]
5. Sun, X.; Li, B.; Lu, H.; Zhong, Y.; Ren, Z.; Lei, Z. Steel/slag interface behavior under multifunction electromagnetic driving in a continuous casting slab mold. *Metals* **2019**, *9*, 983. [CrossRef]
6. Li, X.; Li, B.; Liu, Z.; Niu, R.; Liu, Y.; Zhao, C.; Huang, C.; Qiao, H.; Yuan, T. Large eddy simulation of multi-phase flow and slag entrapment in a continuous casting mold. *Metals* **2018**, *9*, 7. [CrossRef]
7. Zhang, W.; Luo, S.; Chen, Y.; Wang, W.; Zhu, M. Numerical simulation of fluid flow, heat transfer, species transfer, and solidification in billet continuous casting mold with M-EMS. *Metals* **2019**, *9*, 66. [CrossRef]
8. Okazawa, K.; Toh, T.; Fukuda, J.; Kawase, T.; Toki, M. Fluid flow in a continuous casting mold driven by linear induction motors. *ISIJ Int.* **2001**, *41*, 851–858. [CrossRef]
9. Hagemann, R.; Schwarze, R.; Heller, H.P.; Scheller, P.R. Model investigations on the stability of the steel-slag interface in continuous casting process. *Metall. Mater. Trans. B* **2013**, *44*, 80–90. [CrossRef]
10. Han, S.W.; Cho, H.J.; Jin, S.Y.; Sedén, M.; Lee, I.B.; Sohn, I. Effects of simultaneous static and traveling magnetic fields on the molten steel flow in a continuous casting mold. *Metall. Mater. Trans. B* **2018**, *49*, 2757–2769. [CrossRef]
11. Cukierski, K.; Thomas, B.G. Flow control with local electromagnetic braking in continuous casting of steel slabs. *Metall. Mater. Trans. B* **2008**, *39*, 94–107. [CrossRef]
12. Cho, S.; Thomas, B.G. Electromagnetic forces in continuous casting of steel slabs. *Metals* **2019**, *9*, 471. [CrossRef]
13. Zhang, L.S.; Zhang, X.F.; Wang, B.; Liu, Q.; Hu, Z.G. Numerical analysis of the influences of operational parameters on the braking effect of EMBr in a CSP funnel-type mold. *Metall. Mater. Trans. B* **2014**, *45*, 295–306. [CrossRef]
14. Xu, L.; Wang, E.; Karcher, C.; Deng, A.; Xu, X. Numerical simulation of the effects of horizontal and vertical EMBr on jet flow and mold level fluctuation in continuous casting. *Metall. Mater. Trans. B* **2018**, *49*, 2779–2793. [CrossRef]
15. Qian, Z.D.; Wu, Y.L. Large eddy simulation of turbulent flow with the effects of DC magnetic field and vortex brake application in continuous casting. *ISIJ Int.* **2004**, *44*, 100–107. [CrossRef]
16. Harada, H.; Takeuchi, E.; Zeze, M.; Tanaka, H. MHD analysis in hydromagnetic casting process of clad steel slabs. *Appl. Math. Modell.* **1998**, *22*, 873–882. [CrossRef]
17. Wang, Q.; Zhang, L. Influence of FC-Mold on the full solidification of continuous casting slab. *JOM* **2016**, *68*, 2170–2179. [CrossRef]
18. Sarkar, S.; Singh, V.; Ajmani, S.K.; Singh, R.K.; Chacko, E.Z. Effect of argon injection in meniscus flow and turbulence intensity distribution in continuous slab casting mold under the influence of double ruler magnetic field. *ISIJ Int.* **2018**, *58*, 68–77. [CrossRef]
19. Chaudhary, R.; Thomas, B.G.; Vanka, S.P. Effect of electromagnetic ruler braking (EMBr) on transient turbulent flow in continuous slab casting using large eddy simulations. *Metall. Mater. Trans. B* **2012**, *3*, 532–553. [CrossRef]
20. Singh, R.; Thomas, B.G.; Vanka, S.P. Large eddy simulations of double-ruler electromagnetic field effect on transient flow during continuous casting. *Metall. Mater. Trans. B* **2014**, *45*, 1098–1115. [CrossRef]
21. Li, Z.; Zhang, L.; Bao, Y.; Ma, D. Numerical simulation on the brake effect of FAC-EMBr and EMBrRuler in the continuous casting mold. *Processes* **2020**, *8*, 1620. [CrossRef]
22. Brackbill, J.U.; Kothe, D.B.; Zemach, C. A continuum method for modeling surface tension. *J. Comput. Phys.* **1992**, *100*, 335–354. [CrossRef]
23. Miao, X.; Timmel, K.; Lucas, D.; Ren, Z.; Eckert, S.; Gerbeth, G. Effect of an electromagnetic brake on the turbulent melt flow in a continuous-casting mold. *Metall. Mater. Trans. B* **2012**, *43*, 954–972. [CrossRef]
24. Menter, F. Zonal two equation k-ω turbulence models for aerodynamic flows. In Proceedings of the 24th Fluid Dynamics Conference, Orlando, FL, USA, 6–9 July 1993.
25. ANSYS Inc. *ANSYS Fluent User's Guide R18*; ANSYS Publisher: Canonsburg, PA, USA, 2018.
26. Cho, M.J.; Kim, I.C.; Kim, S.J.; Kim, J.K. 3-D Turbulent heat and fluid flow analysis with solidification under the electro-magnetic field. *Trans. Kor. Soc. Mech. Eng. B* **1999**, *23*, 1491–1502.
27. Moreau, R.J. *Magnetohydrodynamics*; Kluwer Academic Pub. Co.: Norwell, MA, USA, 1990; pp. 158–160.